



Modeling the influence of hydroperiod and vegetation on the cross-sectional formation of tidal channels

Andrea D'Alpaos^{a,*}, Stefano Lanzoni^a, Simon Marius Mudd^b, Sergio Fagherazzi^c

^a Dipartimento di Ingegneria Idraulica, Marittima Ambientale e Geotecnica and International Centre for Hydrology "Dino Tonini", University of Padova, Italy

^b Department of Civil and Environmental Engineering, Vanderbilt University, Nashville, TN, USA

^c Department of Geological Sciences and School of Computational Science, Florida State University, Tallahassee, FL, USA

Received 6 April 2006; accepted 2 May 2006

Abstract

The evolution of the cross section of a salt-marsh channel is explored using a numerical model. Deposition on the marsh platform and erosion and deposition in the channel affect the tidal prism flowing through the cross section, such that the model captures the evolution of the stage–discharge relationship as the channel and marsh platform evolve. The model also captures the growth of salt-marsh vegetation on the marsh platform, and how this vegetation affects flow resistance and the rate of sedimentation. The model is utilized to study the influence of hydroperiod and vegetation encroachment on channel cross section. Numerical results show that a reduction in hydroperiod due to the emergence of the marsh platform causes an infilling of the channel. Vegetation encroachment on the marsh surface produces an increase in flow resistance and accretion due to organic and mineral sedimentation, with important consequences for the shape of the channel cross section. Finally, modeling results indicate that in microtidal marshes with vegetation dominated by *Spartina alterniflora*, the width-to-depth ratio of the channels decreases when the tidal flats evolve in salt marshes, whereas the cross-sectional area remains proportional to the tidal peak discharge throughout channel evolution.

© 2006 Published by Elsevier Ltd.

Keywords: tidal channel; salt-marsh vegetation; tidal flats; hydroperiod; coastal geomorphology

1. Introduction

Salt marshes are common in intertidal zones, and are composed of platforms dissected by a network of tidal creeks that transport both water and sediment onto and away from a vegetated surface populated by a limited number of macrophyte species such as *Spartina alterniflora* and *Juncus roemerianis*. The hydrodynamics of these environments depends on the structure and density of tidal creeks (e.g., Fagherazzi et al., 1999; Rinaldo et al., 1999a,b; Marani et al., 2003), while sedimentation rates vary as a function of the distance from

the channel, thus linking sediment transport processes to network morphology and drainage density (e.g., Christiansen et al., 2000; Leonard et al., 2002; Temmerman et al., 2003a,b). Similarly, the composition and distribution of salt-marsh macrophytes depends on the characteristics of the channel network since they play an important role in several edaphic factors, such as nutrient fluxes and soil salinity (Sanderson et al., 2000).

A number of authors have studied the strictly intertwined nature of salt marshes and tidal channels cutting through them. Several models have been proposed to investigate the zero-dimensional growth of salt marshes, where the sedimentation on the marsh platform is a function of sediment supply and either marsh elevation (e.g., Krone, 1987; French, 1993; Allen, 1994, 1995, 1997; Temmerman et al., 2003a) or

* Corresponding author.

E-mail address: adalpaos@idra.unipd.it (A. D'Alpaos).

115 biomass (Randerson, 1979; Morris et al., 2002). The differ-
 116 ential accretion of the marsh platforms, induced by the spatial
 117 variability of sediment deposition rates, as a function of the
 118 distance from the creek, has also been analyzed (Woolnough
 119 et al., 1995; Mudd et al., 2004; Temmerman et al., 2004).
 120 The development of tidal channels and, more generally, the
 121 morphodynamics of tidal networks, have been explored both
 122 in the field (e.g., Pestrong, 1965; Gardner and Bohn, 1980;
 123 Steel and Pye, 1997) and with conceptual and numerical
 124 models (e.g., Yapp et al., 1916, 1917; Beeftink, 1966; French
 125 and Stoddart, 1992; French, 1993; Allen, 2000; Fagherazzi
 126 and Furbish, 2001; Fagherazzi and Sun, 2004; D'Alpaos
 127 et al., 2005). In general, the evolution of a tidal creek is
 128 enhanced by small perturbations in the topography on an
 129 antecedent surface subject to tidal fluxes, which could be
 130 a mud flat or a terrestrial region that is being encroached by
 131 salt water due to sea-level rise (e.g., Allen, 2000; Gardner
 132 and Porter, 2001). As perturbations grow, water flow concen-
 133 trates within the incipient channel, favoring an increase of
 134 the shear stresses and, therefore, erosion within the channel,
 135 which widens and deepens (Steel and Pye, 1997). However,
 136 a feedback mechanism exists which relates the time evolution
 137 of cross-sectional geometry (Friedrichs, 1995; Fagherazzi and
 138 Furbish, 2001) to the vertical growth of the salt-marsh
 139 platform, which tends to reduce the tidal prism and, as a con-
 140 sequence, enhances channel infilling. The flow velocity and
 141 shear stress distribution within tidal channels are, in fact,
 142 determined in large part by the size of the tidal prism which
 143 flows into and out of the intertidal zone (e.g., Pethick, 1980;
 144 Allen, 2000).

145 Field investigators have noted that the above evolutionary
 146 scenario is strongly influenced by the presence of vegetation
 147 which affects not only the planimetric evolution of tidal
 148 channels (e.g., Garofalo, 1980; Gabet, 1998) but also flow
 149 characteristics (e.g., Kadlec, 1990; Leonard and Luther,
 150 1995; Nepf, 1999; Mudd et al., 2004) and sedimentation
 151 processes (e.g., Gleason et al., 1979; Randerson, 1979;
 152 Yang, 1998; Leonard et al., 2002; Morris et al., 2002). For
 153 example, the rate at which water can propagate onto and drain
 154 from the platform adjacent to a channel is influenced by the
 155 drag caused by the stems of macrophytes living upon it
 156 (Nepf, 1999), which increases linearly with plant density
 157 (Lopez and Garcia, 2001). As a direct consequence, flow speed
 158 in the marsh canopy is inversely related to stem density so that
 159 the volume of water transported as a sheet flow on the marsh
 160 platform considerably decreases when vegetation is present
 161 (Leonard and Luther, 1995). Vegetation also favors particle
 162 settling and consequent platform accretion by a reduction of
 163 turbulence levels within the canopy (Leonard and Luther,
 164 1995; Christiansen et al., 2000). However, these studies do
 165 not investigate the response of unvegetated tidal channel cross
 166 sections to vegetation encroachment on the marsh platform.

167 In this paper, we focus on the long-term evolution of the
 168 channel cross section, starting from the initial channel forma-
 169 tion within a tidal flat, with particular emphasis to the role
 170 played by hydroperiod and vegetation. In order to investigate
 171 the driving factors which lead to the observed cross-sectional

172 geometry, we track the growth of the emergent marsh platform
 173 coupled to the evolving morphology of the tidal channel. To
 174 this end, we extend the analysis of Fagherazzi and Furbish
 175 (2001), by considering water levels and flow discharges vari-
 176 able in time, resulting from a quasi-static propagation of the
 177 tide within a given intertidal area, and accounting for the
 178 reduction of the tidal prism after the emergence of the marsh
 179 surface, and for the effects of vegetation on surface drag and
 180 sediment deposition. Furthermore we assume a constant value
 181 for the suspended sediment concentration across the section
 182 which bears as consequence that the deposition of sediments
 183 at the surface is directly proportional to the hydroperiod.

184 The new model can then follow the time evolution of tidal
 185 channels, not only on youthful marshes like those studied by
 186 Fagherazzi and Furbish (2001), but also at late stages of marsh
 187 evolution, when the marsh is emergent. In order to quantify the
 188 effects of vegetation encroachment on channel cross section
 189 we consider the case of a particular species of macrophytes,
 190 *Spartina alterniflora*, using the empirical data gathered from
 191 North Inlet Estuary, South Carolina (Morris and Haskin,
 192 1990; Morris et al., 2002), and the approach of Mudd et al.
 193 (2004) and Palmer et al. (2004) to model the influence of
 194 such a species on tidal flow and sedimentation. The data
 195 will be used to determine the model parameters.

196 A series of two simulations are presented. The first set of
 197 simulations analyzes the influence that marsh-platform
 198 vertical accretion and channel cross-sectional evolution exert
 199 on each other, and how the hydroperiod and, therefore, the
 200 final cross-sectional configuration are affected by this inter-
 201 twined interaction. Inorganic sediment deposition is modeled
 202 as a linear function of the hydroperiod, following the zero-
 203 dimensional formulation of a number of authors (e.g., Krone,
 204 1987; Woolnough et al., 1995; Allen, 1997). In the second
 205 set of simulations, we take into account the role exerted by
 206 *Spartina alterniflora* on the sedimentation rate on the
 207 platform as a function of the biomass of the macrophytes
 208 on the marsh following the approach of Mudd et al.
 209 (2004). The influence of vegetation encroachment on channel
 210 cross-sectional shape is therefore analyzed and discussed.

211 The paper is organized as follows: in Section 2 we describe
 212 the methods used to build the model and its structure, the
 213 assumptions adopted to describe the hydrodynamics, sediment
 214 transport processes, and the effect of vegetation. Section 3
 215 then presents the main results obtained by applying the model
 216 under different scenarios. A discussion section where we
 217 compare significant geomorphic features of the modeled cross
 218 sections to the ones of observed tidal channels and a set of
 219 conclusions close the paper.

2. Methods

2.1. The hydrodynamic model

225 We analyze the morphodynamic evolution of a generic
 226 cross section composed of a tidal channel and an adjacent
 227 marsh platform (e.g., the transect B–C shown in Fig. 1) which
 228 drains a sub-basin of area *A*, whose extent can be determined

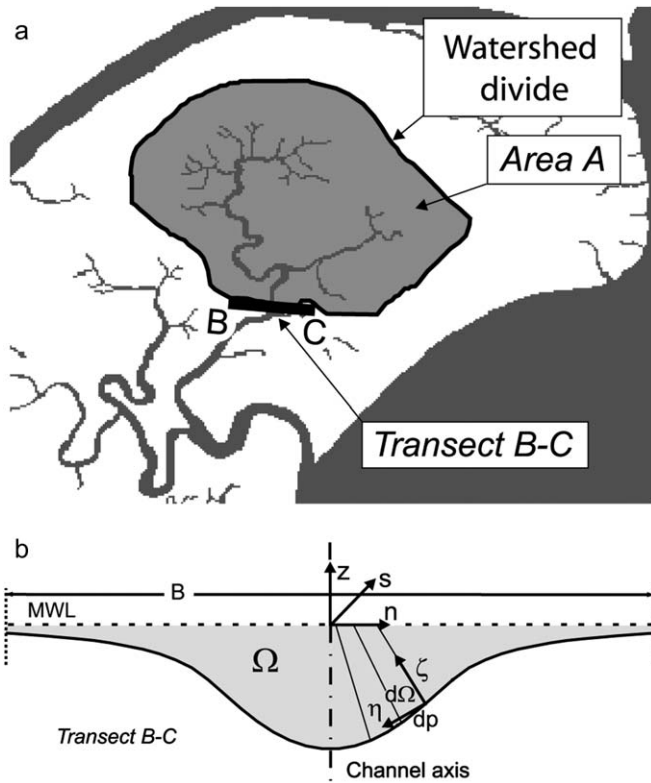


Fig. 1. (a) Portion of the tidal basin (in gray) drained by the considered cross section (B–C). The tidal watershed of area A and its divide is delineated by using the procedure proposed by Rinaldo et al. (1999a) and refined by Marani et al. (2003); (b) typical salt-marsh cross-sectional configuration investigated through the model and notation. The origin of the n, s, z coordinate system is located at the intersection of channel axis and the mean sea level (MSL, which is assumed equal to 0). Note that the spacing between normals to the bottom is greatly exaggerated.

through the procedure proposed by Rinaldo et al. (1999a) and refined by Marani et al. (2003). We assume that the initial bottom configuration of the sub-basin is characterized by a nearly flat surface, with an average elevation well below the minimum low water level (MLWL). For the sake of simplicity, we also assume that the tidal sub-basin has a rectangular shape, and is characterized by a width B and by an upstream length L . The bidimensional model proposed by Fagherazzi and Furbish (2001) simulates the evolution in time of any tidal-flat or salt-marsh transect for given values of the water level and of the flow discharge. In the present contribution we relax such an assumption by considering time varying water levels and flow discharges, resulting from a quasi-static propagation of the tide within the area A closed by the reference cross section under investigation (Fig. 1). At every instant t of the tidal cycle, the discharge flowing through the transect B–C is then calculated following the static model introduced by Boon (1975) and Pethick (1980):

$$Q(t) = \frac{dV}{dt} = \frac{d}{dt}[A(t)D_0(t)] \quad (1)$$

where $A(t)$ is the time-dependent liquid (horizontal) area of the intertidal surface drained by the considered cross section, $V(t)$

is the instantaneous volume of water over the intertidal surface, $D_0(t)$ is the instantaneous mean water depth over the cross section, calculated as $h(t) - z_b(t)$, with $h(t)$ and $z_b(t)$ the instantaneous water and mean bottom elevations over a reference datum, respectively. It is important to note that the drainage area, $A(t)$, is equal to the entire intertidal area (BL) drained by the considered cross section when the domain is completely inundated, but it reduces to its submerged portion ($B_{\text{wet}}L$, where B_{wet} denotes the width of the wetted portion of the transect) when part of the intertidal surface emerges. In our simplified approach, in fact, we do not account for water volume variations related to either the upstream funneling of the channel section and the longitudinal gradients of marsh surface elevation. Such an assumption is justified by the fact that, usually, the convergence length of tidal creeks tends to be larger than the length of the tidal sub-basin (Marani et al., 2002) and that the landward bottom aggradation of the areas flanking the channel is quite small.

At each time step, the oscillating discharge calculated through Eq. (1) is used to evaluate the repartition of bottom shear stresses. Following the procedure introduced by Pizzuto (1990) in the context of gravel rivers, the local value of the bottom shear stress, τ_0 , reads:

$$\tau_0 = \rho g S \frac{d\Omega}{dp} + \frac{d}{dp} \int_0^{D_\zeta} \tau_{\zeta s} d\zeta \quad (2)$$

where ρ is the water density, g is the gravitational acceleration, S is the energy slope, $d\Omega$ the cross-sectional area between two normals to the bed, dp is the wetted perimeter related to $d\Omega$, ζ is a local spatial coordinate normal to the bottom, D_ζ is the total distance along ζ from the bed to the water surface, and $\tau_{\zeta s}$ is the bottom shear stress acting on planes orthogonal to ζ and directed seawards (see Fig. 1b for notation). For details on how Eq. (2) was derived and utilized to model the cross-sectional evolution of salt-marsh channels see Pizzuto (1990) and Fagherazzi and Furbish (2001).

Boundary conditions need to be carefully specified in order to solve Eq. (2). When the entire cross section is unvegetated, the velocity profile along the normal, introduced in order to evaluate $\tau_{\zeta s}$, can be assumed to be logarithmic. Two (identical, for symmetry reasons) boundary conditions are then imposed at the two ends of the transect, associated with the watershed divides, delimiting the drainage area, A (see Fig. 1b), namely:

$$\tau_0 = \rho g S D \quad n = \pm B/2 \quad (3)$$

where D is the local water depth. Note that such boundary conditions have very little effect on the overall stress distribution over B during the cross-sectional evolution, even though they influence the stress near $n = \pm B/2$.

The assumption of a logarithmic velocity distribution along the normal to the bottom, ζ , does not apply when the marsh surface becomes vegetated. As clearly demonstrated by field measurements and experiments carried out by Leonard and Luther (1995) and by Nepf and Vivoni (2000), the velocity

343 distribution is strongly affected by the presence of vegetation,
344 and a logarithmic profile is likely to be attained only above the
345 canopy.

346 Therefore, Eq. (2) can be applied only on the unvegetated
347 portions of the cross-section, which are basically located in
348 the deeper central part, considering a reduced value of the
349 flow discharge. We then impose the boundary conditions (3)
350 on τ_0 , at the edge between the vegetated and unvegetated
351 area, rather than at the endpoints of the transect. The shear
352 stresses on the vegetated portion of the cross section, which
353 are used uniquely to estimate the erosion/deposition rates,
354 are evaluated by retaining only the first term on the right
355 hand side of Eq. (2).

356 Indeed, the second term on the right hand side of Eq. (2),
357 which is responsible for momentum redistribution, has little
358 effect on the shear stress spatial distribution when the bed is
359 nearly horizontal, as on the marsh platform.

360 In order to account for the discharge redistribution which
361 occurs as soon as vegetation starts to encroach on the marsh
362 surface, the discharges flowing, respectively, through the cen-
363 tral unvegetated part of the transect and through the rougher
364 vegetated portions of the cross-section, are calculated by using
365 the procedure proposed by Englund (1966). In particular, in
366 the presence of vegetation, the friction coefficient to be used
367 in the Darcy-Weisbach flow resistance relationship can be
368 evaluated by considering the results of recent experimental
369 studies by Nepf (1999), relating the bulk plant drag coefficient
370 to the product of the projected plant area per unit volume, a_s ,
371 and the stem diameter, d_s , which, as it will be discussed later,
372 can be easily related to plant biomass (Mudd et al., 2004).

373 The bulk drag coefficient, c_D , can then be written as:

$$374 \quad c_D = \alpha_{c_D} b + c_{D0} \quad (4)$$

375 where c_{D0} is the drag coefficient without vegetation, b is the
376 biomass and α_{c_D} is a fitting parameter which links the biomass
377 to the drag coefficient (Mudd et al., 2004). The one-dimen-
378 sional balance between gravity and drag forces allows one to
379 obtain the friction coefficient, f , which has to be used in the
380 Darcy-Weisbach flow resistance relationship, namely:

$$383 \quad f = 4c_D a_s D \quad (5)$$

384 where a_s is the projected plant area per unit volume, and D is
385 the local water depth.

387 Finally, we note that, at a given instant, the energy slope S
388 appearing in Eq. (2), is calculated iteratively, by imposing that
389 the total discharge flowing through the transect equals Q . We
390 start with a guessed value of S , compute the shear stress and
391 flow velocity distributions, we then calculate the correspond-
392 ing discharge Q , if it is higher (lower) than the actual value
393 (determined through Eq. (1)) we reduce (increase) S until
394 convergence (see also Fagherazzi and Furbish, 2001). This is
395 an approximation because actual velocities, energy slope and
396 water depth are related together through the continuity and
397 momentum equations. However, our aim is not to fully
398 describe the flow field caused by tidal motion within an inter-
399 tidal cross-sectional area, but rather to provide a simplified

geomorphological model able to capture the main features of
the cross-sectional evolution of tidal channels.

2.2. Sediment erosion and deposition

We assume the bottom sediment to be cohesive, an assump-
tion consistent with field observations. Evolution of bed
topography is governed by the sediment continuity equation
which can be written in the form:

$$(1 - \lambda) \frac{\partial z_b}{\partial t} = Q_d - Q_e \quad (6)$$

where z_b is the bottom elevation, λ is void fraction in the bed,
and Q_d and Q_e are the deposition and the erosion fluxes,
respectively, representing sediment mass exchange rates, per
unit area, between the water column and the bed.

Many mathematical formulations have been proposed for
 Q_d and Q_e . Here a formulation which can be applied when
the bed properties are relatively uniform over the depth and
the bed is consolidated (Mehta, 1984) is used:

$$Q_e = Q_{e0} \frac{\tau_0 - \tau_c}{\tau_c}, \tau_0 > \tau_c \quad (7)$$

where τ_0 is the local value of the bottom shear stress evaluated
through Eq. (2), τ_c is the cohesive shear stress strength with
respect to erosion, and Q_{e0} is a constant empirical erosion
rate which depends on sediment properties.

As far as the deposition rate is concerned, various sedimenta-
tion mechanisms have to be considered, namely:

$$Q_d = Q_{ds} + Q_{dt} + Q_{db} \quad (8)$$

where Q_{ds} is the deposition rate due to settling, Q_{dt} is the
sedimentation rate due to the trapping effect of the plant
canopy, and Q_{db} is the belowground net organic production
due to plant roots and rhizomes. If the marsh is not vegetated,
both sediment trapping and below ground organic production
are identically zero.

The deposition due to particle settling acts even without the
presence of vegetation and is the chief process responsible for
marsh accretion. To estimate Q_{ds} , the model uses the formula-
tion of Einstein and Krone (1962):

$$Q_{ds} = w_s C_b \left(1 - \frac{\tau_0}{\tau_d} \right), \tau_0 < \tau_d \quad (9)$$

where w_s is the settling velocity that depends on the size of the
estuarine sediment flocs (Gibbs, 1985), τ_d is the shear stress
below which all initially suspended sediment eventually
deposits, C_b is the volumetric sediment concentration at the
bottom, which, following Parker et al. (1987), can be written
as $C_b = rC_0$, with r an empiric coefficient ($r \cong 2$), and C_0
the depth-averaged volumetric concentration of sediments in
the water column.

We consider a bottom composed of fine sediment, which is
transported mainly in suspension. The values typically attained
across the section by the Rouse number ($Z = w_s k^{-1} u_*^{-1}$, with k

the von Karman constant, and u_* the friction velocity) are small enough ($\cong 0.02$ in our simulations) to assume that the sediment is well mixed across the water column. Moreover, the ratio of the horizontal to the vertical length scale is quite large, thus ensuring that the horizontal diffusion of sediment can be neglected with respect to the horizontal advection.

Mathematical modeling of suspended sediment transport carried out by Pritchard and Hogg (2003) indicates that, away from the shoreline, the depth-averaged concentration of suspended sediment tends to a constant value which, generally, is a function of the threshold velocities for erosion and deposition. In our simulations we then assume that the suspended sediment concentration in the water column is constant across the section and throughout the simulation. Note that this assumption is widely utilized in zero-dimensional models that focus on the interplay between salt-marsh accretion and sea-level rise (Krone, 1987; Allen, 1994). Moreover, with the assumption of constant sediment concentration, the deposition of sediments at the surface is directly proportional to the hydroperiod, so that for mature marshes the rate of marsh accretion decreases and the marsh elevation tends toward an asymptotic value that corresponds to mean high tide (Pethick, 1981).

For emergent salt marshes the vegetation encroachment at the surface increases the amount of sediment deposited due to the trapping effect of plant stems and leaves and the reduction of turbulence due to vegetation. Nepf (1999) demonstrated the reduction in turbulence caused by plant stems using laboratory experiments. Leonard and Luther (1995) and Leonard et al. (2002) found that turbulent energy within vegetated canopies on marsh platforms were much smaller than the turbulent energies in marsh creeks. Others have found turbulence to be a primary influence of sediment transport in intertidal areas (e.g., French et al., 1993).

The above studies suggest that the amount of sediment trapped is proportional to the concentration of suspended sediment and to the number of plant stems that can both reduce the turbulent energy and capture sediment particles. Following Palmer et al. (2004), we express the trapping rate as follows:

$$Q_{dt} = C_0 u \eta d_s n_s h_s \quad (10)$$

where u is a typical value of the flow speed through vegetation, η is the rate at which transported sediment particles are captured by plant stems, d_s is the stem diameter, n_s is the stem density per unit area, and h_s is the average height of the stems. The capture efficiency η reads:

$$\eta = \alpha_\eta \left(\frac{u d_s}{\nu} \right)^{\beta_\eta} \left(\frac{d_p}{d_s} \right)^{\gamma_\eta} \quad (11)$$

where d_p is particle diameter, ν is the kinematic viscosity of the water, α_η , β_η , and γ_η are empirical coefficients obtained by Palmer et al. (2004).

Finally, the belowground production of organic matter can be directly linked to the biomass following the work of Randerson (1979):

$$Q_{db} = Q_{db0} \frac{b}{b_{\max}} \quad (12)$$

where b_{\max} is the maximum value of the biomass, and Q_{db0} is a typical deposition rate which is derived empirically from field measurements. For example Blum and Christian (2004), report a maximum organic sediment accretion of about 9 mm/year for a *Spartina alterniflora* marsh in Virginia. In reality the belowground storage of organic material in salt marshes is an extremely complex process that involves root production, microbial decomposition, as well as edaphic factors such as nutrients availability and salinity (Blum and Christian, 2004; Cahoon et al., 2004) which are not considered in our simplified approach.

2.3. Vegetation parameterization

Eqs. (4), (5), (10)–(12) require the estimate of plant biomass, b , as well as of several parameters related to it as: η , d_s , n_s , h_s , Q_{db0} and b_{\max} . In the present contribution we focus on the case of salt marshes characterized by a prevailing presence of *Spartina alterniflora*, a species of halophytic vegetation quite common in tidal environments. Long-term field studies on the physiology of a *S. alterniflora* community at North Inlet estuary, South Carolina, have been carried out by Morris and Haskin (1990) and Morris et al. (2002). The observed data show that the biomass of *S. alterniflora* can be related (Mudd et al., 2004) to the differences $z_{\max} - z_b$ and $z_{\max} - z_{\min}$, where z_{\max} is the maximum elevation withstood by *S. alterniflora*, z_{\min} is the minimum value at which vegetation starts to encroach the surface, and z_b is the local marsh elevation. The duration of inundation, in fact, will decrease as z_b increases, thus affecting soil salinity because evapotranspiration concentrates salts in pore water if the marsh is not regularly flooded (Morris, 1995). A number of researchers have shown that increased pore water salinity caused by evapotranspiration can limit growth or be fatal to salt-marsh macrophytes (e.g., Phleger, 1971; Webb, 1983; Morris, 2000). While other biotic and abiotic factors may be important in determining plant productivity (see Silvestri and Marani, 2004, and references therein), following the approach adopted by Mudd et al. (2004), based on the long record of plant productivity at North Inlet, we relate the vegetation biomass to the platform elevation z_b with respect to z_{\max} and z_{\min} , namely:

$$b_{ps} = \begin{cases} 0 & z_b < z_{\min} \\ \frac{b_{\max}}{z_{\max} - z_{\min}} (z_{\max} - z_b) & z_{\min} \leq z_b \leq z_{\max} \\ 0 & z_b > z_{\max} \end{cases} \quad (13)$$

where b_{ps} is the biomass as a function of marsh elevation in g/m^2 , and b_{\max} is the maximum biomass.

Furthermore, to account for the seasonal variability in biomass, which usually peaks during the summer months, the biomass is corrected using the equation (Morris and Haskin, 1990):

$$b = \frac{b_{ps}(1 - \omega)}{2} \left[\sin \left(\frac{2\pi m}{12} - \frac{\pi}{2} \right) + 1 \right] + \omega b_{ps} \quad (14)$$

with $m = 1, 12$ the month ($m = 1$ corresponds to January) and ω a dimensionless factor that accounts for the reduction in biomass during the winter months (Mudd et al., 2004).

Finally, the fitting of the data collected by Morris and Haskin (1990), indicates that the stem density per unit area, n_s , and the average height of the stems, h_s , can be expressed as a function of plant biomass (Mudd et al., 2004):

$$n_s = \alpha_n b^{\beta_n} \quad (15)$$

$$h_s = \alpha_h b^{\beta_h} \quad (16)$$

where α_n , β_n , α_h and β_h are empirical coefficients.

Analogously, the projected plant area per unit volume, a_s , and the stem diameter, d_s , can be cast as (Mudd et al., 2004):

$$a_s = \alpha_a b^{\beta_a} \quad (17)$$

$$d_s = \alpha_d b^{\beta_d} \quad (18)$$

where α_a , β_a , α_d and β_d are empirical coefficients.

2.4. Simulation setup

Two distinct sets of simulations have been carried out. The first series analyzes how the hydroperiod is influenced by the intertwined interaction between marsh-platform vertical growth and channel formation, and how such processes affect channel cross-sectional evolution, without taking into account for the growth of vegetation on the emerging marshes. The second series analyzes the effect of vegetation on flow resistance, sediment trapping, production of organic soil and,

therefore, on channel formation and cross-sectional evolution. In both cases we assume that the volumetric concentration of sediments transported in suspension, C_0 , is constant across the section and equal to 20 mg/l during the entire tidal cycle.

We consider a tidal sub-basin (see, e.g. Fig. 1), characterized by a cross section of width $B = 200$ m, and a landward length $L = 1000$ m, having therefore a drainage area of 2.0×10^5 m². The initial bottom elevation is $z_{b0} = -1.00$ m below mean sea level (MSL). A forcing semidiurnal sinusoidal tide characterized by an amplitude equal to 0.74 m above MSL is assumed, so that at the beginning of the simulation, the bottom is submerged during the entire tidal cycle. This approach is taken in order to simulate the emergence of a marsh platform from a tidal mud flat. We consider fine cohesive sediments with characteristics reported in Table 1. In particular, since we are interested in the long-term morphological evolution of the marsh cross section, the critical bottom shear stresses for erosion, τ_e , and deposition, τ_d , are those characterizing fully consolidated mud (Pritchard, 2001). Table 1 also shows the values of the parameters necessary to evaluate the various terms in the sediment continuity equation (i.e., Eq. (6)). *Spartina alterniflora* is assumed to be the dominant vegetation species which colonizes the emerged salt-marsh surfaces. In all runs we start from a deep, flat, and unchanneled initial bottom configuration with a small incision (1.0 cm) in correspondence of the longitudinal axis of the computational domain, to favor channel initiation at that location.

3. Model results

The main results of the first series of simulations are shown in Figs. 2–4. Fig. 2 portrays the time evolution of the channel cross-sectional geometry (Fig. 2a) and of the relative distribution of bottom shear stresses (Fig. 2b), together with the time evolution of the bottom elevation in correspondence of the channel axis and of a point located on the salt marsh (Fig. 2c). It clearly appears that, during the initial stages of the morphodynamic evolution, the threshold value for erosion, τ_e , is nowhere exceeded within the cross section (Fig. 2a,b;

Table 1
Parameters used in the simulations

Parameter	Value	Ref.	Parameter	Value	Ref.
τ_e	0.4 N/m ²	Parchure and Mehta (1985)	α_a	0.25	Mudd et al. (2004)
τ_d	0.1 N/m ²	Parchure and Mehta (1985)	β_a	0.5	Mudd et al. (2004)
ρ_s	2600 kg/m ³		α_d	0.0006	Gibbs (1985)
w_s	2×10^{-4} m/s	Gibbs (1985)	β_d	0.3	Fagherazzi and Furbish (2001)
D_{50}	50 μ m		α_n	250	Mudd et al. (2004)
λ	0.4		β_n	0.3032	Mudd et al. (2004)
Q_{e0}	3.0×10^{-4} kg/m ² s	Fagherazzi and Furbish (2001)	α_h	0.0609	Gibbs (1985)
C_0	20 mg/l	Mudd et al. (2004)	β_h	0.1876	Fagherazzi and Furbish (2001)
R	2.0	Mudd et al. (2004)	α_{cd}	0.224	Mudd et al. (2004)
α_η	0.224	Palmer et al. (2004)	c_{d0}	0.718	Mudd et al. (2004)
β_η	0.718	Palmer et al. (2004)	z_{min}	0.14 m	Morris et al. (2002)
γ_η	2.08	Palmer et al. (2004)	z_{max}	0.72 m	Morris et al. (2002)

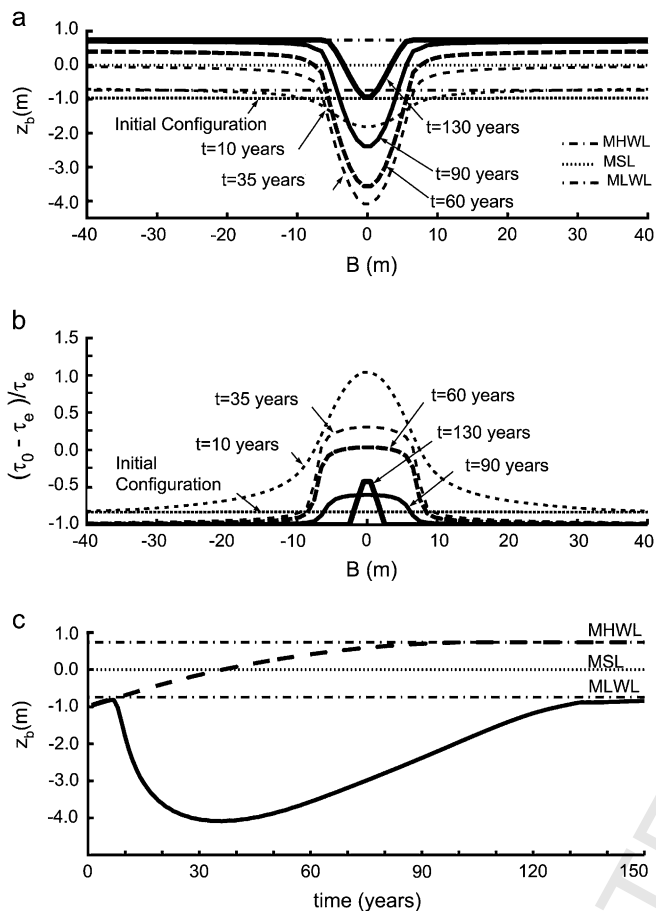


Fig. 2. Evolution in time of (a) cross-sectional bottom elevations and (b) relative distributions of the maximum bottom shear stresses through a tidal cycle, in and near the channel, and evolution in time of (c) the elevation of the channel axis (solid line) and of a point located on the marsh surface (dashed line), in the unvegetated scenario. Mean high water level (MHWL), mean sea level (MSL), and mean low water level (MLWL) are also indicated.

initial configuration). However, the progressive increase in bottom elevation associated to deposition leads to shear stress values greater than τ_e over a part of the cross section, in particular at points closer to the channel axis, where the initial bottom incision is located. A small primary drainage channel characterized by shelving banks develops (Fig. 2a: $t=10$ years). Flux begins to concentrate within the channel after

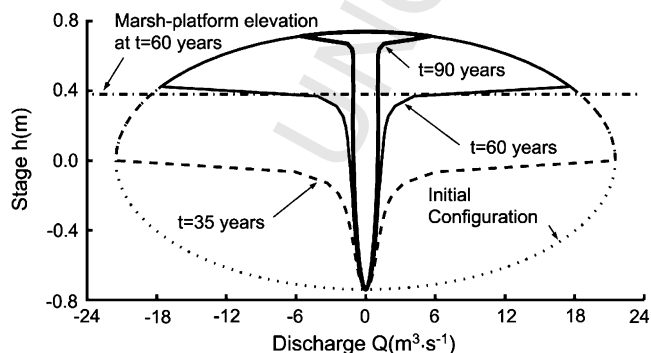


Fig. 3. Stage–discharge relationship during the tidal cycle at different stages of channel development. Mean marsh-platform elevation at $t=60$ years is also indicated (dash-dot line).

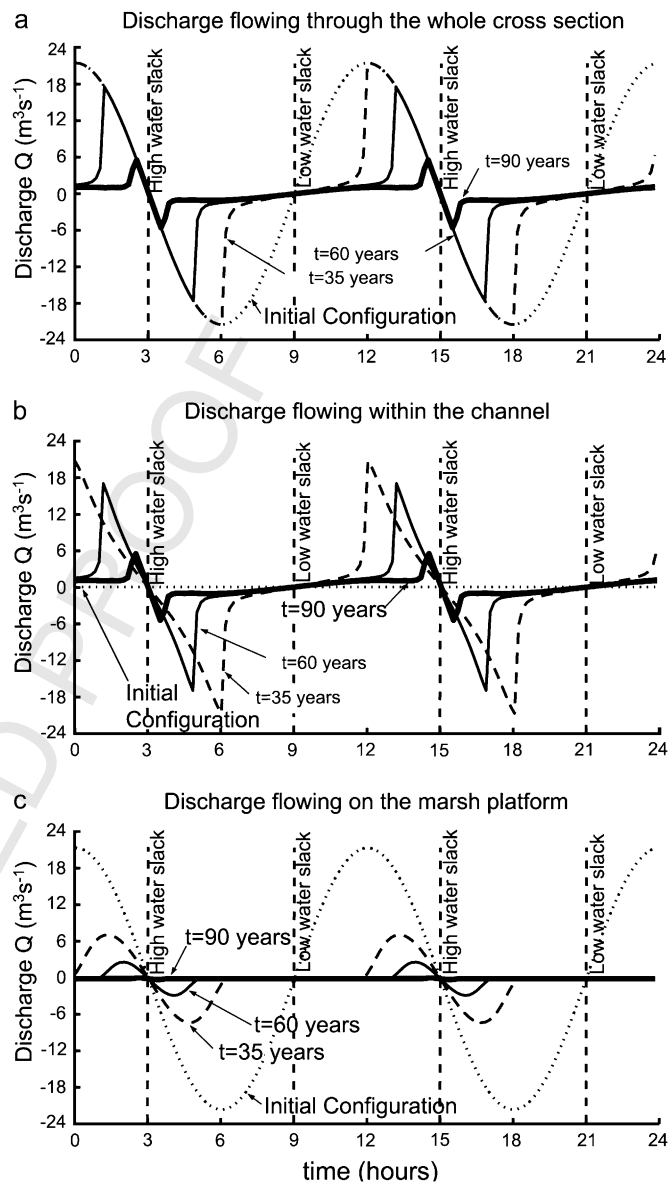


Fig. 4. Discharge–time relationship during the tidal cycle at different stages of channel development. (a) Discharge flowing through the whole cross section; (b) discharge flowing within the channel; (c) discharge flowing on the marsh platform.

its formation due to its increasing cross-sectional area and decreasing flow resistance that is the result of an increase in the depth of flow within the channel. The increased flow velocity associated to the reduction of the relative bottom roughness in the channel with respect to the adjacent marsh platform leads to higher bottom shear stresses and, consequently, to erosion and deepening of the channel, creating a feedback mechanism between erosion and channel formation. On the marsh surface adjacent to the channel, the flow velocity is everywhere decreasing to maintain the discharge equal to the one prescribed by Eq. (1) (Fig. 2b: $t=10$ years). As channel depth increases, both through bed erosion and by accretion of the adjoining marsh platform, the shelving slopes of the channel are transformed into steeper banks (Fig. 2a: $t=35$ years). As the marsh platform grows above mean sea level,

799 a reduction in the maximum discharge is observed as a conse-
 800 quence of the reduction of the tidal prism due to the
 801 emergence of part of the tidal sub-basin. Deposition tends to
 802 prevail over erosion and the channel starts silting thus increas-
 803 ing its average bed elevation and decreasing its width (Fig. 2a:
 804 $t > 35$ years). The shape of the resulting cross section,
 805 composed of a high level marsh with a well developed chan-
 806 nel, is dictated by the succession of the landscape-forming
 807 discharges that the channel has experienced. At the end of
 808 the simulation, since the marsh surface is close to high tide
 809 level, overbank fluxes are rare and only tidal fluxes confined
 810 within the channel prevent its silting. The final channel geom-
 811 etry (Fig. 2a: $t = 130$ years) stems thus from a delicate balance
 812 between erosion and deposition.

813 The above evolutionary scenario is clearly confirmed by
 814 Fig. 2c, which shows the time evolution of the bottom eleva-
 815 tion in correspondence of the channel axis (solid line) and
 816 of a point located on the salt marsh, where erosion is negligi-
 817 bly small (dashed line). It appears that the channel axis
 818 deepens as long as the marsh platform lies below mean sea
 819 level. As soon as the marsh platform gets higher than mean
 820 sea level, two combined processes modify the morphological
 821 evolution of the marsh. The reduction in hydroperiod progres-
 822 sively slows deposition over the marsh platform, whose
 823 elevation tends asymptotically to mean high water level, in
 824 accordance with observational evidence put forth by Pethick
 825 (1981). Meanwhile the reduction in tidal prism reduces the
 826 tidal discharges in the channel and the related shear stresses,
 827 favoring the infilling of the channel.

828 The reduction of the maximum value attained by the flow
 829 discharge during the tidal cycle, when the elevation of the
 830 marsh platform becomes higher than mean sea level, is illus-
 831 trated in Fig. 3, which reports some typical examples of the
 832 stage–discharge relationship at different stages of the morpho-
 833 logical evolution. When the marsh platform is submerged
 834 during the entire tidal cycle, the curve is symmetrical with
 835 respect to the mean water level. The drainage area, A , to the
 836 considered cross section, in fact, does not vary in time
 837 ($B_{\text{wet}} = B$), and maximum flood and ebb discharges occur
 838 when dh/dt is maximum or minimum, respectively (i.e.,
 839 when the water elevation $h = 0$). On the other hand, when
 840 the marsh surface emerges, the maximum value of the
 841 discharge tends to decrease, the reduction being progressively
 842 enhanced as the marsh elevation increases. The maximum
 843 flood and ebb discharges are attained when the time derivative
 844 of the product $A(t)D_0(t)$ is maximum. The stage–discharge
 845 relationship provided by the model qualitatively agrees with
 846 observational evidence (e.g., Myrick and Leopold, 1963;
 847 Bayliss-Smith et al., 1978; Healey et al., 1981; French and
 848 Stoddard, 1992), even if the model, when considering a
 849 sinusoidal forcing, cannot capture the asymmetries of such a
 850 relationship which are typically observed in tidal landscapes.
 851 In particular, for basins with marshlands that fully dry during
 852 a tidal cycle, maximum flood discharge occurs after the tide
 853 exceeds bank-full elevation and inundates the marsh surface,
 854 while, on the contrary, maximum ebb discharge occurs below
 855 bank-full elevation (Healey et al., 1981).

Also the shape of the discharge–time curves is influenced
 by the movement of water across the marsh surface, as shown
 in Fig. 4 which illustrates discharge–time curves at different
 stages of the process of channel development. The discharges
 flowing through the whole cross section (curves in Fig. 4a),
 within the channel (curves in Fig. 4b), and on the marsh
 edge (curves in Fig. 4c), all exhibit the typical shape observed
 in tidal environments (Rinaldo et al., 1999b; Lawrence et al.,
 2004). If we impose harmonic changes in water elevation as
 seaward boundary condition and we neglect tidal current
 asymmetry and distortion, arising from nonlinear effects as
 the wave propagates from the inlet towards the inner part of
 the basin, the discharge flowing through the whole cross
 section (curve relative to the initial configuration in Fig. 4a)
 is harmonic as well, as long as the elevation of the marsh plat-
 form is lower than the minimum water elevation during a tidal
 cycle (see Eq. (1)). When the elevation of the salt-marsh
 surface increases due to sedimentation, the bottom topography
 becomes important and topographic nonlinearities affect the
 discharge–time relationship, which then loses its harmonic
 behavior (curves relative to $t = 35, 60$ and 90 years in
 Fig. 4a). At the beginning of the simulation, when the tidal
 creek has not yet formed, the discharge flowing through the
 whole cross section coincides with the discharge flowing on
 the marsh platform (compare curves relative to the initial
 configuration in Fig. 4a and c). As the channel develops and
 the elevation on the marsh platform increases, the discharge
 is mainly conveyed within the channel (Fig. 4b) and only
 a small amount of water flows across the marsh platform
 (Fig. 4c).

The main results of the second series of simulations, taking
 into account the effects of vegetation, are shown in Figs. 5–9.
 The evolution in time of the cross-sectional geometry, the
 stage–discharge relationship and the discharge–time curves
 are qualitatively similar to those obtained for the unvegetated

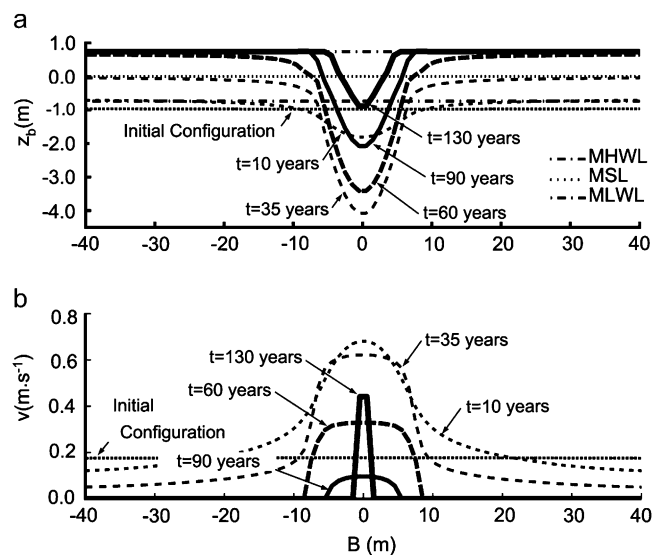


Fig. 5. Evolution in time of (a) cross-sectional bottom elevations and (b) relative distributions of the maximum velocities through a tidal cycle, in and near the channel, in the vegetated scenario.

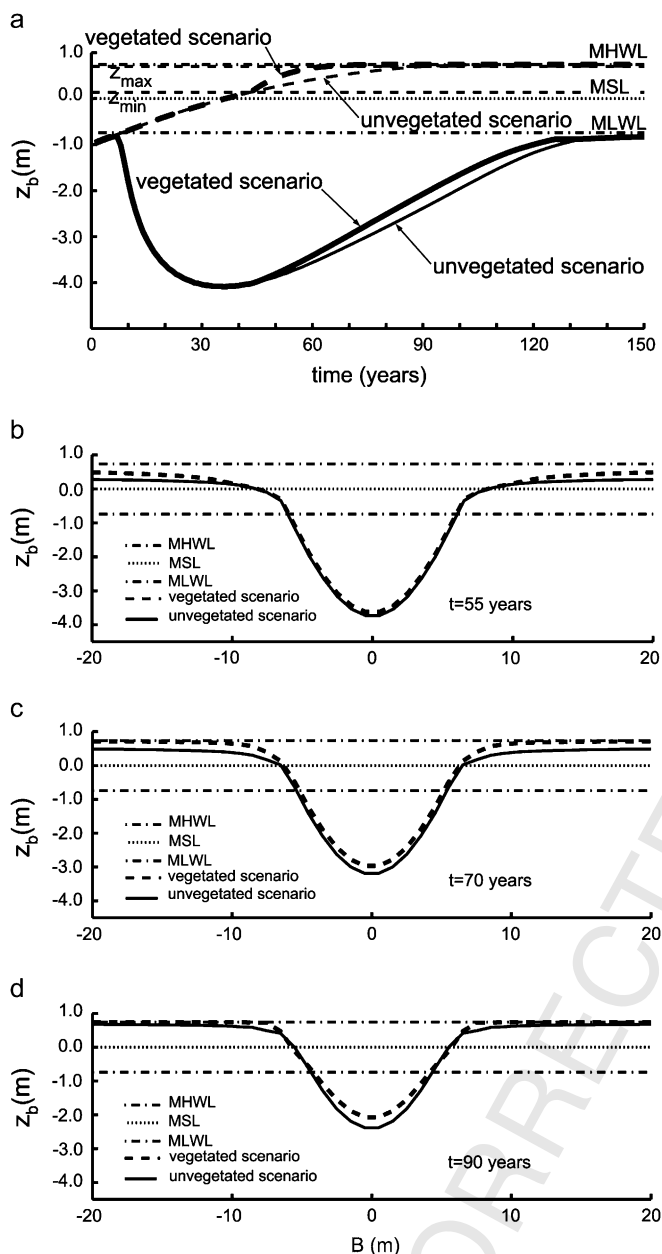


Fig. 6. (a) Comparison of the time evolution of bottom elevation in correspondence of the channel axis (solid lines) and of a point located on the salt marsh (dashed lines), in absence (thin lines) or in presence of vegetation (bold lines); (b,c,d.) channel cross sections at different stages of channel development (b: $t=55$ years; c: $t=70$ years; d: $t=90$ years), in the absence (solid lines) or in the presence of vegetation (dashed lines). Mean high water level (MHWL), mean sea level (MSL), and mean low water level (MLWL) are also indicated, together with the vegetation parameters z_{\min} and z_{\max} .

case. Nevertheless, some important differences arise, which need to be discussed. Fig. 5 portrays an example of the time evolution of the cross-sectional geometry (Fig. 5a) and of the relative distribution of maximum flow velocity (Fig. 5b), in the case of a vegetated marsh. As long as the marsh platform is not encroached by vegetation, not surprisingly, cross-sectional bottom configurations (Fig. 5a) show exactly the same behavior as in the unvegetated case (Fig. 2a). However, as soon as vegetation starts populating the marsh surface,

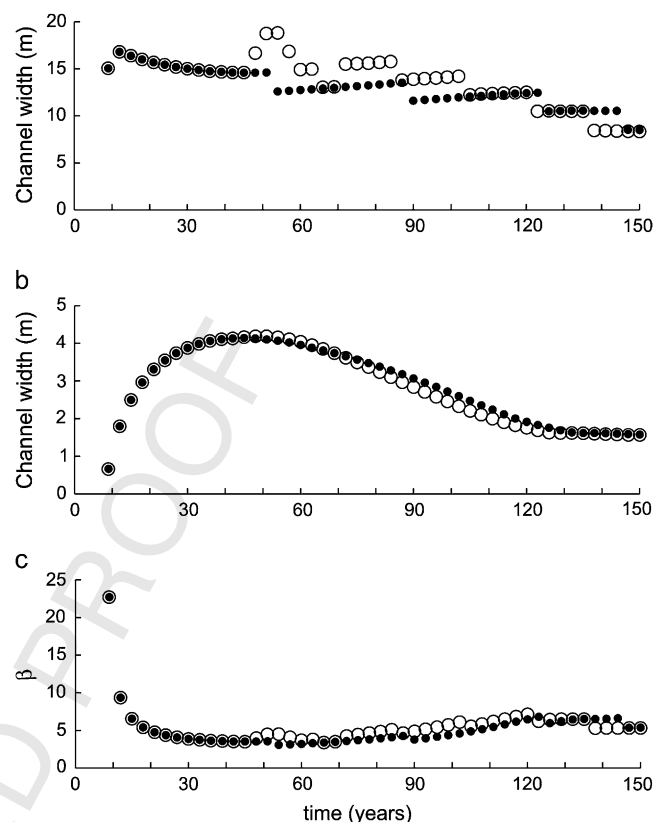


Fig. 7. (a) Channel width, (b) channel depth, and (c) width-to-depth ratio, β , at different stages of channel development, in the absence (solid circles) or in the presence of vegetation (open circles). The channelled portion of the cross section has been evaluated by coupling bed elevation and curvature threshold criteria, in analogy with Fagherazzi et al. (1999). Channel points are those in which $|c| > 0.1 \text{ m}^{-1}$ or $z_{\text{marsh}} - z < 0.3 \text{ m}$, where c and z are, respectively, the curvature and the elevation of the considered point, and z_{marsh} is the average marsh-platform elevation.

it influences both sediment transport processes and flow dynamics. The vertical growth of the marsh platform is enhanced by the increased inorganic sediment deposition due to trapping effects of the canopy and by the deposition of organic sediment (Fig. 5a, $t \geq 35$ years). The velocities on the marsh platform are strongly reduced (Fig. 5b) as well as the discharge flowing on the vegetated part of the cross section. As a consequence, the flow tends to be more concentrated within the channel, increasing the amount of water flowing through it, as to maintain an overall discharge equal to the one prescribed by Eq. (1) (Fig. 5b, $t \geq 35$ years). However, our results suggest that, if vegetation begins to grow when flow velocities on the marsh surface are already very slow, the increased flow within the channel might not be strong enough to modify the section shape (Fig. 5b).

Such an observation is reinforced by Fig. 6. In particular, Fig. 6a shows a comparison of the time evolution of the bottom elevation in correspondence of the channel axis and of a point located on the salt marsh, in the absence or in the presence of vegetation. It clearly appears that vegetation growth modifies the evolution of both the channel bottom and the marsh surface (Fig. 6a). Indeed, the increased deposition rate associated to vegetation trapping and organic

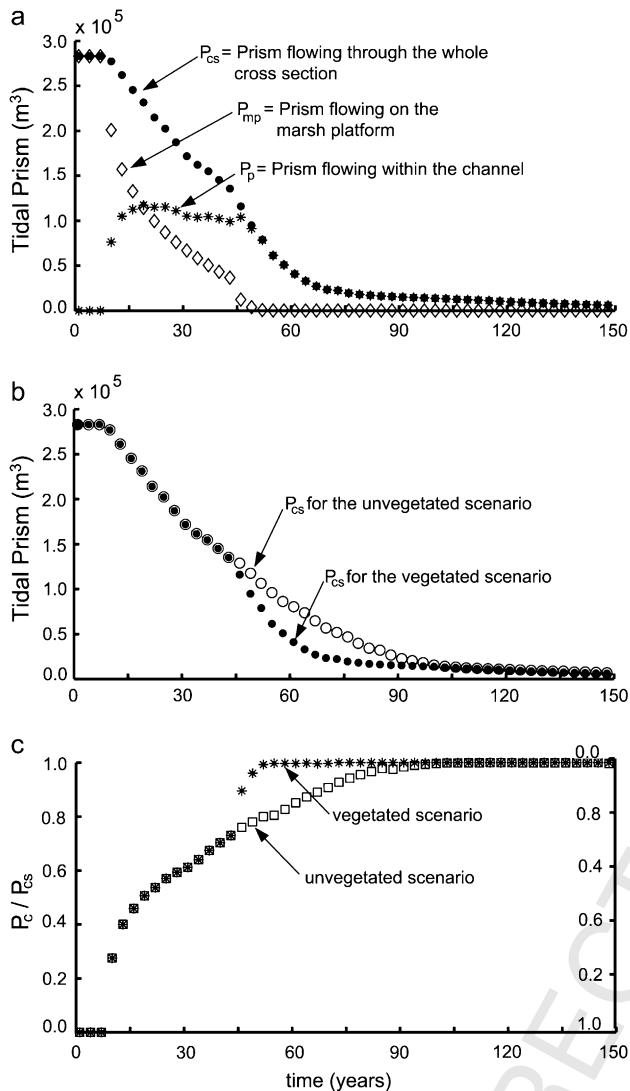


Fig. 8. (a) Repartition of total tidal prism flowing through the whole cross section, P_{cs} in tidal prism flowing within the channel, P_c , and on the marsh platform, P_{mp} estimated through the model at different stages of the evolution. (b) Comparison between P_{cs} values at different stages of the evolution, in the presence or in the absence of vegetation. (c) Comparison between the ratios P_c/P_{cs} and P_{mp}/P_{cs} at different stages of the evolution, in the presence or in the absence of vegetation.

production leads to a faster growth of the marsh platform than in the unvegetated case and, accordingly, to a more rapid reduction in the maximum discharges (see e.g. Fig. 3) which counteracts the “concentration” of discharge within the channel induced by the enhanced resistance on the vegetated areas. Therefore, the channel starts infilling more rapidly, as shown also in Fig. 6b–d, which portrays a comparison between bottom configurations at corresponding stages ($t = 55, 70, 90$ years, respectively), in the unvegetated and vegetated scenarios. Furthermore, it should be noted that in presence of vegetation, the transition between channel banks and adjacent salt-marsh platform tends to become more abrupt.

A comprehensive view of the evolution in time of channel width (evaluated by coupling bed elevation and curvature threshold criteria, in analogy with Fagherazzi et al., 1999),

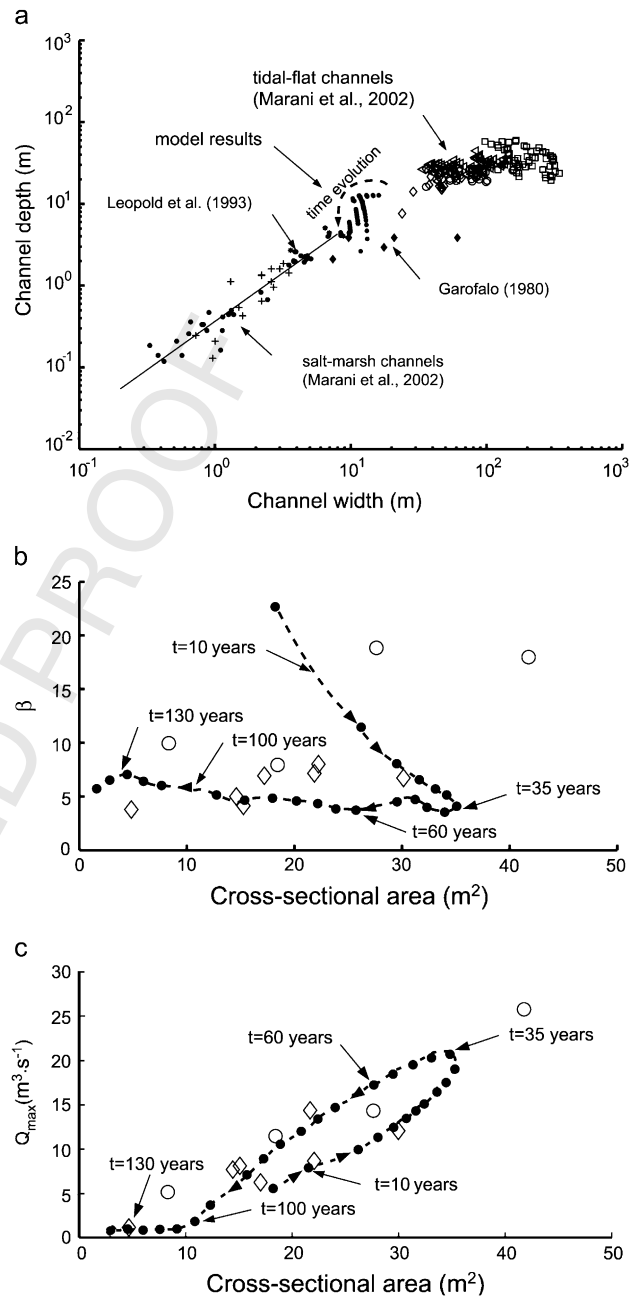


Fig. 9. (a) Calculated channel width versus depth and field data derived from measurements of tidal channels in New Jersey, USA (Garofalo, 1980), San Francisco Bay, USA (Leopold et al., 1993), and in the Venice Lagoon, Italy (Marani et al., 2002). The evolutionary trend of the model results is also shown; (b) evolution in time of the width-to-depth ratio, β , as a function of cross-sectional area, Ω , computed with reference to MSL; (c) evolution in time of maximum flow discharge, Q_{max} , as a function of cross-sectional area, Ω , computed with reference to the MSL. Observed data derived from measurements of tidal channels by Garofalo (1980) (open circles) and Leopold et al. (1993) (diamonds) are also indicated.

channel depth, and width-to-depth ratio, β , is depicted in Fig. 7. Even though the vegetated and unvegetated trends of the above quantities are similar, nonetheless, it emerges that soon after vegetation growth the channel experiences a little widening (Fig. 7a), and, owing to differential accretion, a more pronounced deepening (Fig. 7b). Such an observation

1141 does not contradict the scenario emerging from Fig. 6a–d. In
1142 fact, even if the channel infills more rapidly, its depth relative
1143 to the marsh surface increases as a consequence of the much
1144 faster accretion rate of the adjoining marsh platform (compare
1145 channel depth values for the vegetated and unvegetated case in
1146 Fig. 7b). The width-to-depth ratio, β , varies in time according
1147 to variations in cross-sectional morphology (Fig. 7c). As the
1148 channel starts forming within the tidal-flat surface its cross
1149 section is characterized by β -values close to 23. A relatively
1150 rapid decrease of β characterizes the next stages of channel
1151 evolution: channel width, in fact, maintains nearly constant
1152 (Fig. 7a), while channel depth increases (Fig. 7b) due to pre-
1153 vailing of erosion. Finally, as the marsh platform emerges
1154 and, consequently, the maximum discharges decrease, β tends
1155 to slightly increase as a consequence of channel silting which
1156 prevails on channel narrowing.

1158 4. Discussion

1160 The static hydrodynamic model described in the previous
1161 sections appears to reproduce a geomorphologically relevant
1162 feature of tidal creek hydrodynamics, namely the significant
1163 decrease in maximum discharges within the channels attained
1164 when tide levels are just below the bank-full elevation and the
1165 marsh platform dries (see Figs. 3 and 4) in accordance with the
1166 field observations carried out by Myrick and Leopold (1963),
1167 Bayliss-Smith et al. (1978), Pethick (1980), and Healey et al.
1168 (1981). Moreover, despite its simplifying assumptions, the
1169 proposed model gives a satisfactory estimate of the tidal
1170 discharge for relatively small tidal basins (Lanzoni and
1171 Seminara, 1998; Fagherazzi, 2002; Fagherazzi et al., 2003),
1172 particularly when the three-dimensional structure of the marsh
1173 is unknown. Obviously, some observed features such as the
1174 asymmetry of the velocities in the creeks when the marsh plat-
1175 form is inundated/drained, and the delay in the velocity peak
1176 after marsh inundation, associated to the strong nonlinearities
1177 produced by wetting and drying, cannot be captured by a static
1178 model (Healey et al., 1981), which presupposes a flat water
1179 surface which moves synchronously with the tidal forcing.

1180 The coupling of the simplified hydrodynamic model with
1181 erosion/deposition relationships and a parametrization of veg-
1182 etation effects, makes it possible to reproduce evolutionary
1183 scenarios which are in accordance with a number of concep-
1184 tual models depicting the intertwined evolution of tidal chan-
1185 nels and the adjoining marsh platform (e.g., Yapp, 1916, 1917;
1186 Beefink, 1966; French and Stoddart, 1992; French, 1993;
1187 Steel and Pye, 1997). In particular, the different stages of
1188 marsh development envisioned by various conceptual models
1189 (see the review by Allen, 2000) are reflected in the simulated
1190 channel cross-sectional evolution. In the initial stages the to-
1191 pographic irregularities of tidal flats influence the morphology
1192 of the forming marsh channels. Indeed, we have shown that
1193 even a small perturbation in the tidal-flat bottom triggers the
1194 formation of a marsh channel as long as the flow concentration
1195 is enough to produce erosion. Intermediate stages of channel
1196 evolution typical of youthful marshes, are characterized by
1197 a progressive deepening and enlarging of the channel. During

1198 the deepening process the channel cuts older deposits remobi-
1199 lizing the sediments. The channel width is established earlier
1200 in the evolution, whereas the depth is more sensitive to
1201 discharge variations, as shown in Fig. 7a,b, indicating that
1202 channel depth varies in a wider range than channel width. In
1203 the final stage the emergence of the marsh platform reduces
1204 significantly the tidal discharges in the channel, so that depo-
1205 sition overcomes erosion. During this phase the channel tends
1206 to be filled, reducing both its width and depth. At the end of
1207 the evolution, when the platform elevation is close to mean
1208 high tide level, the contribution of the marsh edge to the total
1209 discharge is negligibly small, and the tidal flux is essentially
1210 confined to the channel (see e.g., Fig. 4). The repartition of
1211 tidal prism between channel and marsh platform along the
1212 cross section $B-C$ estimated through the model at different
1213 stages of evolution is shown in Fig. 8. When the marsh begins
1214 to emerge ($t = 35$ years), most of the discharge is concentrated
1215 within the channel, which accounts for 60% of the discharge,
1216 in agreement with the numerical results of Lawrence et al.
1217 (2004) and the measurements of French and Stoddart (1992)
1218 for a U.K. marsh characterized by a mean high water level
1219 of 0.8 m (Lawrence et al., 2004), above the marsh platform,
1220 i.e., similar to the calculated configuration attained after 35
1221 years. However, Fig. 8a indicates that as the channel further
1222 develops and the marsh platform vertically grows, the total
1223 tidal prism flowing through the whole cross section decreases
1224 and gets more and more concentrated within the channel,
1225 while the tidal prism flowing on the marsh surface is strongly
1226 reduced.

1227 As far as the effects of vegetation on the tidal prism are
1228 concerned, Fig. 8b clearly shows that the reduction in time
1229 of the total tidal prism is enhanced by the vegetation en-
1230 croachment. This is due to the fact that the marsh platform
1231 grows more rapidly because of the increased deposition of
1232 organic and inorganic sediment. The presence of vegetation,
1233 also induces an increase in flow resistance and, therefore,
1234 favors the concentration of discharge within the channel.
1235 However, as shown in Fig. 8c, in our simulations such an in-
1236 crease is experienced “late” in the process of cross-sectional
1237 evolution, i.e., when the maximum discharges shaping the
1238 channel have already been considerably reduced (see also
1239 Figs. 3 and 4a,b).

1240 Vegetation encroachment on the marsh surface is thus
1241 found to produce two competing effects. On the one hand,
1242 the increase in flow resistance on the marsh platform concen-
1243 trates the flow in the channel, leading to a possible channel
1244 overdeepening. On the other hand, vegetation also favors
1245 deposition of both organic and inorganic material, thus
1246 increasing the platform elevation with a reduction in tidal
1247 prism and related discharges, resulting in channel infilling.
1248 Our simulations suggest that the second process is more
1249 important during marsh evolution, because the further concen-
1250 tration of flux within the channel due to vegetation encroach-
1251 ment occurs at a later stage of marsh accretion, when most of
1252 the flow is already confined to the channel. Obviously, the
1253 situation might be different when vegetation colonizes the
1254 surface at lower elevations or when the tidal signal is strong

1255 enough to move large volumes of water on the marsh surface,
1256 as it happens in the macrotidal U.K. marshes.

1257 The evolutionary trend exhibited by the width-to-depth
1258 ratio, depicted in Fig. 7, suggests that the cross-sectional
1259 geometry tends to evolve from an initial configuration typical
1260 of tidal-flat channels (characterized by larger values of β)
1261 towards a final configuration resembling salt-marsh creeks
1262 (characterized by smaller values of β). This behavior is appar-
1263 ent also in Fig. 9a, reporting calculated channel width versus
1264 depth values, as well as observed data derived from measure-
1265 ments of tidal channels in *Spartina* marshes in New Jersey
1266 (Garofalo, 1980), San Francisco Bay (Leopold et al., 1993),
1267 and in tidal flats and salt marshes (with a mix of vegetation
1268 species) in the Venice Lagoon, Italy (Marani et al., 2002).
1269 All these three environments are characterized by a tidal
1270 excursion comparable to the one adopted in our model.

1271 The calculated values not only are compatible with
1272 observed features, but also suggest an evolutionary trend
1273 according to which both channel width and depth continuously
1274 reduce as the intertidal areas flanking the channel progres-
1275 sively grow and become vegetated, transforming the tidal
1276 flat into a salt marsh. Such a picture is confirmed by the
1277 time evolution of the relationship between β , and the cross-
1278 sectional area, Ω , computed with reference to MSL, shown
1279 in Fig. 9b. In the early stages of channel development β rapidly
1280 decreases while Ω increases until the marsh-platform elevation
1281 becomes greater than the MSL. The subsequent reduction of
1282 the landscape-forming discharges (see e.g., Fig. 3) then leads
1283 to a progressive decrease of the cross-sectional area, which,
1284 however, maintains a nearly constant value of β . It might be
1285 worthwhile to note that the ranges experienced by β and Ω
1286 during the section evolution resulting from our simulation
1287 are in agreement with the values typical of observed sections
1288 (Garofalo, 1980; Leopold et al., 1993).

1289 Finally, the time evolution of the relationship between peak
1290 discharge and cross-sectional area, shown in Fig. 9c, suggests
1291 that the average channel velocity remains nearly constant
1292 during channel evolution, as long as the marsh platform is
1293 significantly lower than mean high water level. The estimated
1294 average channel velocity turns out to be roughly 0.5 m/s,
1295 a value consistent with field data observations of Garofalo
1296 (1980) and Leopold et al. (1993). We can then infer that during
1297 the transition from tidal flats to salt marshes, although the
1298 channel shape changes in time, reducing its width with respect
1299 to the depth, a nearly linear relationship holds between cross-
1300 sectional area and peak discharge, thus indicating that the cross
1301 section adapts quite rapidly to changes in water discharge.

1302 Further studies are deemed necessary to incorporate
1303 important processes acting on salt marshes: time-dependent
1304 deposition as a function of platform elevation (Temmerman
1305 et al., 2003a); spatial gradient of sedimentation rates that in-
1306 crease the accretion near the channel and produce levees
1307 (Woolnough et al., 1995; Mudd et al., 2004; Temmerman
1308 et al., 2004); vegetation zonation (Silvestri and Marani,
1309 2004); and bank collapse linked to meander evolution and
1310 geotechnical properties of the sediments (Gabet, 1998;
1311 Fagherazzi et al., 2004).

5. Conclusions

The model results presented herein are potentially applicable only to microtidal marshes with a uniform *Spartina* canopy. Nonetheless, they provide insights into tidal channel morphology and evolution that are of general interest. The main conclusions of our simulations can be summarized as follows:

- Deposition on tidal flats progressively reduces the water depth and increases the bottom shear stresses, promoting erosion. Topographic irregularities enhance flux concentration at given locations, leading to bottom erosion and the formation of a channel in which the flow further concentrates, thus increasing channel dimensions in a self-sustained process.
- A reduction in hydroperiod after the emergence of the marsh platform causes an infilling of the channel due to the reduced discharge, and an asymptotic growth of the marsh elevation, caused by a decreased deposition rate.
- Vegetation encroachment on the marsh surface produces two competing effects. On the one hand, the increased flow resistance on the canopy promotes the concentration of the flow within the channel, leading to channel over-deepening. On the other hand, enhanced marsh accretion associated to vegetation reduces the tidal prism and the hydroperiod, thus resulting in channel infilling. Our simulations indicate that the second process is more important in microtidal marshes dominated by *Spartina alterniflora*, where the vegetation encroachment occurs when most of the tidal flux is already confined in the channel.
- At the beginning of the simulation the tidal exchanges with the ocean occur as sheet flow on the tidal-flat surface. When the tidal flat emerges and becomes a salt marsh, most of the flow is concentrated within the channel, which accounts for more than 60% of the tidal prism. Finally, in a mature salt marsh (elevation higher than 30 cm above MSL) more than 90% of the tidal prism is confined in the channel. Furthermore the increase in friction driven by vegetation encroachment favors the concentration of flow in the channel.
- The temporal variability of channel depth is higher than the variability of channel width, suggesting that changes in tidal prism most likely produce bottom infilling—scouring rather than channel widening—narrowing. As a consequence, the aspect ratio changes during channel evolution, and, in particular, during the transition from tidal flats to salt marshes.
- The ratio between peak discharge and cross-sectional area (i.e., the maximum average velocity in the channel) remains nearly constant during channel evolution. Therefore, although the shape of the cross section depends on channel history, its area is dictated by the tidal prism and related discharges.

Acknowledgments

Funding from: the Office of Naval Research, award n. N00014-05-1-0071, the Center for Earth Surface Processes

Research (CESPR), Florida State University; the TIDE EU RTD Project (EVK3-2001-00064); 2001 ASI project Dinamica degli ambienti a marea; 2001 MURST 40% Idrodinamica e Morfodinamica a Marea; CORILA (Consorzio per la Gestione del Centro di Coordinamento delle Attività di Ricerca inerenti il Sistema Lagunare di Venezia) (Research Program 2000–2004, Linea 3.2 Idrodinamica e Morfodinamica Linea 3.7 Modelli Previsionali); and Fondazione Ing. A. Gini are gratefully acknowledged.

References

- Allen, J.R.L., 1994. A continuity-based sedimentological model for temperate-zone tidal salt marshes. *Journal of the Geological Society of London* 151, 41–49.
- Allen, J.R.L., 1995. Salt-marsh growth and fluctuating sea level: Implications of a simulation model for Holocene coastal stratigraphy and peat-based sea-level curves. *Sedimentary Geology* 113, 21–45.
- Allen, J.R.L., 1997. Simulation models of salt-marsh morphodynamics: some implications for high-intertidal sediment couplets related to sea-level change. *Sedimentary Geology* 113 (3–4), 211–223.
- Allen, J.R.L., 2000. Morphodynamics of Holocene salt marshes: a review sketch from the Atlantic and Southern North Sea coasts of Europe. *Quaternary Science Review* 19 (17–18), 1155–1231.
- Bayliss-Smith, T.P., Healey, R., Lailey, R., Spencer, T., Stoddart, D.R., 1978. Tidal flows in salt-marsh creeks. *Estuarine and Coastal Marine Science* 9, 235–255.
- Beefink, W.G., 1966. Vegetation and habitat of the salt marshes and beach plains in the south-western part of The Netherlands. *Wentia* 15, 83–108.
- Boon III, J.D., 1975. Tidal discharge asymmetry in a salt marsh drainage system. *Limnology and Oceanography* 20, 71–80.
- Blum, L.K., Christian, R.R., 2004. Belowground production and decomposition along a tidal gradient in a Virginia salt marsh. In: Fagherazzi, S., Marani, M., Blum, L.K. (Eds.), *The Ecogeomorphology of Salt Marshes*. Estuarine and Coastal Studies Series. American Geophysical Union, pp. 47–74.
- Cahoon, D.R., Ford, M.A., Hensel, P.F., 2004. Ecogeomorphology of *Spartina patens*-dominated tidal marshes: soil organic matter accumulation, marsh elevation dynamics, and disturbance. In: Fagherazzi, S., Marani, M., Blum, L.K. (Eds.), *The Ecogeomorphology of Salt Marshes*. Estuarine and Coastal Studies Series. American Geophysical Union, pp. 247–266.
- Christiansen, T., Wiberg, P.L., Milligan, T.G., 2000. Flow and sediment transport on a tidal salt marsh surface. *Estuarine, Coastal and Shelf Science* 50 (3), 315–331.
- D'Alpaos, A., Lanzoni, S., Marani, M., Fagherazzi, S., Rinaldo, A., 2005. Tidal network ontogeny: channel initiation and early development. *Journal of Geophysical Research* 110, F02001. doi:10.1029/2004JF000182.
- Einstein, H.A., Krone, R.B., 1962. Experiments to determine modes of cohesive sediment transport in salt water. *Journal of Geophysical Research* 67 (4), 1451–1461.
- Englund, F., 1966. Hydraulic resistance of alluvial streams. *ASCE* 92 (HY 2), 315–326.
- Fagherazzi, S., Bortoluzzi, A., Dietrich, W.E., Adami, A., Marani, M., Lanzoni, S., Rinaldo, A., 1999. Tidal networks 1. Automatic network extraction and preliminary scaling features from digital terrain maps. *Water Resources Research* 35 (12), 3891–3904.
- Fagherazzi, S., Furbish, D.J., 2001. On the shape and widening of salt marsh creeks. *Journal of Geophysical Research* 106 (C1), 991–1005.
- Fagherazzi, S., 2002. Basic flow field in a tidal basin. *Geophysical Research Letters* 29 (8). doi:10.1029/2001GL013787.
- Fagherazzi, S., Wiberg, P.L., Howard, A.D., 2003. Tidal flow field in a small basin. *Journal of Geophysical Research* 108 (C3), 3071. doi:10.1029/2002JC001340.
- Fagherazzi, S., Gabet, E.J., Furbish, D.J., 2004. The effect of bidirectional flow on tidal platforms. *Earth Surface Processes and Landforms* 29, 295–309.
- Fagherazzi, S., Sun, T., 2004. A stochastic model for the formation of channel networks in tidal marshes. *Geophysical Research Letters* 31. doi:10.1029/2004GL020965.
- Friedrichs, C.T., 1995. Stability shear-stress and equilibrium cross-sectional geometry of sheltered tidal channels. *Journal of Coastal Research* 11 (4), 1062–1074.
- French, J.R., Stoddart, D.R., 1992. Hydrodynamics of salt-marsh creek systems – implications for marsh morphological development and material exchange. *Earth Surface Processes and Landforms* 17 (3), 235–252.
- French, J.R., 1993. Numerical-simulation of vertical marsh growth and adjustment to accelerated sea-level rise, North Norfolk, UK. *Earth Surface Processes and Landforms* 18 (1), 63–81.
- French, J.R., Clifford, N.J., Spencer, T., 1993. High frequency flow and suspended sediment measurements in a tidal wetland channel. In: Clifford, N.J., French, J.R., Hardisty, J. (Eds.), *Turbulence: Perspectives on Flow and Sediment Transport*. Wiley, pp. 249–277.
- Gabet, E.J., 1998. Lateral migration and bank erosion in a salt marsh tidal channel in San Francisco Bay, California. *Estuaries* 21 (4B), 745–753.
- Gardner, L.R., Bohn, M., 1980. Geomorphic and hydraulic evolution of tidal creeks on a subsiding beach ridge plain, North-Inlet, Sc. *Marine Geology* 34 (3–4), M91–M97.
- Gardner, L.R., Porter, D.E., 2001. Stratigraphy and geologic history of a southeastern salt marsh basin, North Inlet, South Carolina, USA. *Wetlands Ecology and Management* 9, 371–385.
- Garofalo, D., 1980. The influence of wetland vegetation on tidal stream migration and morphology. *Estuaries* 3, 258–270.
- Gibbs, R.J., 1985. Estuarine flocs – their size, settling velocity and density. *Journal of Geophysical Research-Oceans* 90 (NC2), 3249–3251.
- Gleason, M.L., Elmer, D.A., Pien, N.C., Fisher, J.S., 1979. Effects of stem density upon sediment retention by salt-marsh cord Grass, *Spartina alterniflora* Loisel. *Estuaries* 2 (4), 271–273.
- Healey, R.G., Pye, K., Stoddart, D.R., Bayliss-Smith, T.P., 1981. Velocity variation in salt marsh creeks, Norfolk, England. *Estuarine, Coastal and Shelf Science* 13, 535–545.
- Kadlec, R.H., 1990. Overland-flow in wetlands – vegetation resistance. *Journal of Hydraulic Engineering – ASCE* 116 (5), 691–706.
- Krone, R.B., 1987. A method for simulating historic marsh elevations. In: Krause, N.C. (Ed.), *Coastal Sediments '87*. American Society of Civil Engineers, New York, pp. 316–323.
- Lanzoni, S., Seminara, G., 1998. On tide propagation in convergent estuaries. *Journal of Geophysical Research* 103, 30793–30812.
- Lawrence, D.S.L., Allen, J.R.L., Havelock, G.M., 2004. Salt marsh morphodynamics: an investigation of tidal flows and marsh channel equilibrium. *Journal of Coastal Research* 20 (1), 301–316.
- Leonard, L.A., Luther, M.E., 1995. Flow hydrodynamics in tidal marsh canopies. *Limnology and Oceanography* 40 (8), 1474–1484.
- Leonard, L.A., Wren, P.A., Beavers, R.L., 2002. Flow dynamics and sedimentation in *Spartina alterniflora* and *Phragmites australis* marshes of the Chesapeake Bay. *Wetlands* 22 (2), 415–424.
- Leopold, L.B., Collins, J.N., Collins, L.M., 1993. Hydrology of some tidal channels in estuarine marshlands near San Francisco. *Catena* 20, 469–493.
- Lopez, F., Garcia, M.H., 2001. Mean flow and turbulence structure of open-channel flow through non-emergent vegetation. *Journal of Hydraulic Engineering – ASCE* 127 (5), 392–402.
- Marani, M., Lanzoni, S., Zandolin, D., Seminara, G., Rinaldo, A., 2002. Tidal meanders. *Water Resources Research* 38 (11), 1225. doi:10.1029/2001WR000404.
- Marani, M., Belluco, E., D'Alpaos, A., Defina, A., Lanzoni, S., Rinaldo, A., 2003. On the drainage density of tidal networks. *Water Resources Research* 39 (2), 105–113.
- Mehta, A., 1984. Characterization of cohesive sediment properties and transport processes in estuaries. In: Mehta, A.J. (Ed.), *Estuarine Cohesive Sediment Dynamics*. Lecture Notes on Coastal And Estuarine Studies, vol. 14. Springer-Verlag, Berlin, pp. 290–315.
- Morris, J.T., Haskin, B., 1990. A 5-yr record of aerial primary production and stand characteristics of *Spartina alterniflora*. *Ecology* 71 (16), 2209–2217.
- Morris, J.T., 1995. The mass balance of salt and water in intertidal sediments: results from North Inlet, South Carolina. *Estuaries* 18, 556–567.

- 1483 Morris, J.T., 2000. Effects of sea level anomalies on estuarine processes. In:
1484 Hobbie, J. (Ed.), Estuarine Science: A Synthetic Approach to Research
1485 and Practice. Island Press, Washington, DC, pp. 107–127.
- 1486 Morris, J.T., Sundareshwar, P.V., Nietch, C.T., Kjerfve, B., Cahoon, D.R.,
1487 2002. Responses of coastal wetlands to rising sea level. Ecology 83,
1488 2869–2877.
- 1489 Mudd, S.M., Fagherazzi, S., Morris, J.T., Furbish, D.J., 2004. Flow, sedimentation,
1490 and biomass production on a vegetated salt marsh in South
1491 Carolina: toward a predictive model of marsh morphologic and ecologic
1492 evolution. In: Fagherazzi, S., Marani, M., Blum, L.K. (Eds.), The Ecogeomorphology of Salt Marshes. Estuarine and Coastal Studies Series. American Geophysical Union, pp. 165–188.
- 1495 Myrick, R.M., Leopold, L.B., 1963. Hydraulics geometry of a small tidal
1496 estuary. U.S. Geological Survey Professional Papers 422-B, 18 pp.
- 1497 Nepf, H.M., 1999. Drag, turbulence, and diffusion in flow through emergent
1498 vegetation. Water Resources Research 35 (2), 479–489.
- 1499 Nepf, H.M., Vivoni, E., 2000. Flow structure in depth-limited, vegetated flow.
1500 Journal of Geophysical Research 105 (C12), 28547–28557.
- 1501 Palmer, M.R., Nepf, H.M., Pettersson, T.J.R., Ackerman, J.D., 2004. Observations of particle capture on a cylindrical collector: implications for particle accumulation and removal in aquatic systems. Limnology and Oceanography 49 (1), 76–85.
- 1505 Parchure, T.M., Mehta, A.J., 1985. Erosion of soft cohesive sediment deposits.
1506 Journal of Hydraulic Engineering – ASCE 111 (10), 1308–1326.
- 1507 Parker, G., Garcia, M.H., Fukushima, Y., Yu, W., 1987. Experiments on turbidity currents over an erodible bed. Journal of Hydraulic Research 25 (1), 123–147.
- 1510 Pethick, J.S., 1980. Velocity surges and asymmetry in tidal channels. Estuarine and Coastal Marine Science 11, 331–345.
- 1511 Pethick, J.S., 1981. Long-term accretion rates on tidal salt marshes. Journal of Sedimentary Petrology 51 (2), 571–577.
- 1514 Pstrong, R., 1965. The development of drainage patterns on tidal marshes. Stanford University Publications, Geological Sciences (Technical Report 10) 87 pp.
- 1517 Phleger, C.F., 1971. Effect of salinity on growth of a salt marsh grass. Ecology 52 (5), 908–911.
- 1519 Pizzuto, J.E., 1990. Numerical simulation of gravel river widening. Water Resources Research 26 (9), 1971–1980.
- 1521 Pritchard, D., 2001. Some problems in two-phase flow: intertidal mudflats and low Reynolds number gravity currents. PhD thesis, University of Bristol.
- 1524 Pritchard, D., Hogg, A.J., 2003. Cross-shore sediment transport and the equilibrium morphology of mudflats under tidal currents. Journal of Geophysical Research 108 (C10), 3313. doi:10.1029/2002JC001570.
- Randerson, P.F., 1979. A simulation model of salt-marsh development and plant ecology. In: Knights, B., Phillips, A.J. (Eds.), Estuarine and Coastal Land Reclamation and Water Storage. Saxon House, Farnborough, pp. 48–67.
- Rinaldo, A., Fagherazzi, S., Lanzoni, S., Marani, M., Dietrich, W.E., 1999a. Tidal networks 2. Watershed delineation and comparative network morphology. Water Resources Research 35 (12), 3905–3917.
- Rinaldo, A., Fagherazzi, S., Lanzoni, S., Marani, M., Dietrich, W.E., 1999b. Tidal networks 3. Landscape-forming discharges and studies in empirical geomorphic relationships. Water Resources Research 35 (12), 3919–3929.
- Silvestri, S., Marani, M., 2004. Salt marsh vegetation and morphology: modeling and remote sensing observations. In: Fagherazzi, S., Marani, M., Blum, L.K. (Eds.), The Ecogeomorphology of Salt Marshes. Estuarine and Coastal Studies Series. American Geophysical Union, pp. 5–26.
- Sanderson, E.W., Ustin, S.L., Foin, T.C., 2000. The influence of tidal channels on the distribution of salt marsh plant species in Petaluma Marsh, CA, USA. Plant Ecology 146 (1), 29–41.
- Steel, T.J., Pye, K., 1997. The development of salt marsh tidal creek networks: evidence from the UK. In: Proceedings of the Canadian Coastal Conference, CCSEA, pp. 267–280.
- Temmerman, S., Govers, G., Meire, P., Wartel, S., 2003a. Modelling long-term tidal marsh growth under changing tidal conditions and suspended sediment concentrations, Scheldt estuary, Belgium. Marine Geology 193 (1–2), 151–169.
- Temmerman, S., Govers, G., Wartel, S., Meire, P., 2003b. Spatial and temporal factors controlling short-term sedimentation in a salt and freshwater tidal marsh, Scheldt estuary, Belgium, SW Netherlands. Earth Surface Processes and Landforms 28 (7), 739–755.
- Temmerman, S., Govers, G., Meire, P., Wartel, S., 2004. Simulating the long-term development of levee-basin topography on tidal marshes. Geomorphology 63, 39–55.
- Webb, J.W., 1983. Soil–water salinity variations and their effects on *Spartina Alterniflora*. Contributions in Marine Science 26 (September), 1–13.
- Woolnough, S.J., Allen, J.R.L., Wood, W.L., 1995. An exploratory numerical-model of sediment deposition over tidal salt marshes. Estuarine, Coastal and Shelf Science 41 (5), 515–543.
- Yang, S.L., 1998. The role of *Scirpus* marsh in attenuation of hydrodynamics and retention of fine sediment in the Yangtze Estuary. Estuarine, Coastal and Shelf Science 47 (2), 227–233.
- Yapp, R.H., Johns, D., Jones, O.T., 1916. The salt marshes of the Dovey Estuary. Part I. Introductory. Journal of Ecology 4, 27–42.
- Yapp, R.H., Johns, D., Jones, O.T., 1917. The salt marshes of the Dovey Estuary. Part II. The salt marshes. Journal of Ecology 5, 65–103.